Mutation of a Novel Gene Results in Abnormal Development of Spermatid Flagella, Loss of Intermale Aggression and Reduced Body Fat in Mice

Patrick K. Campbell,[*,†] Katrina G. Waymire,[‡] Robb L. Heier,[†,‡] Catherine Sharer,[§,] Diane E. Day,[**,††] Heike Reimann,[‡‡] J. Michael Jaje,[‡] Glenn A. Friedrich,[§§,1] Margit Burmeister,[***] Timothy J. Bartness,[**,††] Lonnie D. Russell,[†††,2] Larry J. Young,[§,**] Michael Zimmer,[‡‡‡] Dieter E. Jenne[‡‡] and Grant R. MacGregor[‡,**,3]**

**Emory University School of Medicine, Atlanta, Georgia 30322, †Graduate Program in Genetics and Molecular Biology, Emory University, Atlanta, Georgia 30322, ‡Center for Molecular Medicine, Emory University School of Medicine, Atlanta, Georgia 30322, §Department of Psychiatry, Emory University, Atlanta, Georgia 30322, **NSF Center for Behavioral Neuroscience, Emory University, Atlanta, Georgia 30322, ††Department of Biology, Georgia State University, Atlanta, Georgia 30303, ‡‡Department of Neuroimmunology, Max Planck Institute of Neurobiology, Martinsried 82152, Germany, §§Department of Molecular and Human Genetics, Baylor College of Medicine, Houston, Texas 77030, ***Mental Health Research Institute, University of Michigan, Ann Arbor, Michigan 48109, †††Department of Physiology, Southern Illinois University School of Medicine, Carbondale, Illinois 62901 and ‡‡‡Institute of Clinical Biochemistry and Pathobiochemistry, University of Würzburg, 97080 Würzburg, Germany*

Manuscript received March 20, 2002
Accepted for publication June 3, 2002

ABSTRACT

ROSA22 male mice are sterile due to a recessive gene-trap mutation that affects development of the spermatid flagellum. The defect involves the flagellar axoneme, which becomes unstable around the time of its assembly. Despite a subsequent complete failure in flagellar assembly, development of the spermatid head appears normal and the spermatid head is released at the correct stage in spermatogenesis. The mutation is pleiotropic. Although ROSA22 homozygote males have normal levels of circulating testosterone and display normal mating behavior, they do not exhibit intermale aggressive behavior and have reduced body fat. The mutated gene (*Gtrgeo22*) maps to mouse chromosome 10 and is closely flanked by two known genes, *Madcam1* and *Cdc34*. Ribonuclease protection analysis indicates that expression of the flanking genes is unaffected by the mutation. *Gtrgeo22* is expressed at low levels in epithelial cells in several tissues, as well as in testis and brain. Analysis of the peptide coding sequence suggests that *Gtrgeo22* encodes a novel transmembrane protein, which contains dileucine and tyrosine-based motifs involved in intracellular sorting of transmembrane proteins. Analysis of the *Gtrgeo22* gene product should provide novel insight into the molecular basis for intermale aggression and sperm flagellar development.

THE flagellum provides the motility required for a spermatozoon to reach and penetrate an egg. Despite its importance in fertilization, the molecular basis for development of the mammalian spermatid flagellum is poorly understood. In part, this is due to the lack of a suitable cell culture system that can be used to study this process. The insolubility of many flagellar proteins has also hampered analysis of flagellar composition. Consequently, much of the current understanding of this intricate developmental process comes from electron micrographic studies of mammalian spermatogenesis (Phillips 1974; Fawcett 1975) as well as analysis of mice with mutations that affect this process (Handel 1987; Cebra-Thomas and Silver 1991).

The motor for the sperm flagellum is provided by the axoneme (9 + 2 microtubule structure). Significant knowledge of axonemal composition and function has been derived from studies using the unicellular biflagellate algae *Chlamydomonas reinhardtii* (Huang *et al.* 1982; Dutcher 1995; Mitchell 2000). Orthologs of several protein components of the Chlamydomonas axoneme have been identified in the mammalian spermatozoon (Patel-King *et al.* 1997; Kagami *et al.* 1998; Neilson *et al.* 1999), which illustrates the conserved nature of this specialized cytoskeletal structure.

The mammalian sperm flagellum is composed of an axoneme surrounded by two predominant accessory structures, the outer dense fibers (ODFs) and the fibrous sheath (FS; Fawcett 1975), each of which is composed of a variety of proteins (O'Brien and Bellve 1980). Although ODFs are found in spermatozoa from

Sequence data from this article have been deposited with the EMBL/GenBank Data Libraries under accession no. AF303106.

[1]*Present address:* Ceros Limited, Cambridge, England.

[2]Deceased July 11, 2001.

[3]*Corresponding author:* Department of Developmental and Cell Biology and Center for Molecular and Mitochondrial Medicine and Genetics, University of California, Irvine, CA 92697-3940.
E-mail: gmacg@uci.edu

a variety of vertebrate and invertebrate species, the FS appears to be unique to mammals (Fawcett 1975). These accessory structures are thought to modulate the bending motion of the flagellum, thereby enhancing its propulsive force (Mortimer 1997). Development of the spermatid flagellum begins immediately after meiosis. In the mouse, the haploid stage of spermatogenesis, termed spermiogenesis, has been classified in 16 steps (Russell *et al.* 1990). Early in step 1 the paired centrioles lie near the plasma membrane. The initial flagellum is a simple axoneme that forms by rapid accretion of microtubules onto the distal centriole (Phillips 1974; Fawcett 1975; Gerton and Millette 1984). The growing axoneme rapidly extends to the lumen of the seminiferous tubule, with growth being completed by steps 2–3 of spermiogenesis (Irons and Clermont 1982b). Formation of the FS commences at steps 2–3 and growth and maturation of the FS and ODFs is completed shortly before spermatid release (spermiation) at step 16 (Irons and Clermont 1982a,b).

Despite the insolubility of many of its proteins, genes for several components of the mammalian flagellum have been cloned using various experimental strategies (Carrera *et al.* 1994; Fulcher *et al.* 1995; O'Bryan *et al.* 1998; Shao *et al.* 2001). This approach has proven successful for proteins of moderate to high abundance, but can be challenging if the gene product is expressed at relatively low levels. In contrast, genetic screens for mutations are unaffected by this issue. Moreover, the mutant phenotype provides direct evidence that the gene product has an essential function in a particular process. We have used retroviral insertional mutagenesis to identify genes whose products have an essential role in mouse spermatogenesis. Homozygous ROSA22 male mice are sterile due to defective sperm flagellar development. The recessive mutation is pleiotropic with two additional striking effects: Adult male mutants do not display intermale aggression and have reduced body fat.

MATERIALS AND METHODS

Mouse husbandry: Generation of the ROSA22 strain has been described (Friedrich and Soriano 1991). In this study, mice were N2 for C57BL/6 (B6) on a hybrid B6, 129S5/SvEvBrd (B6/129S5) background. More recently, ROSA22 mice have been crossed onto congenic B6 and 129S4 backgrounds. ROSA22 mutants on either a congenic or a 129B6 F_1 background display essentially identical phenotypes. Animals were housed in micro-isolator cages. Purina 5021 mouse chow and acidified water were provided *ad libitum*. Light cycle was off 8 p.m./on 7 a.m.

PCR genotyping: DNA was isolated from tail tips as described (Hogan *et al.* 1994). For PCR genotyping reactions, DNA was amplified in 30-μl reactions containing 0.5 mm dNTPs, 0.5 μm forward primer, 0.25 μm each reverse primer, 1.5 mm $MgCl_2$, and 1 unit of *Taq* polymerase (Promega, Madison, WI) in the buffer supplied with the enzyme. Reaction conditions were 35 cycles of 95°, 45 sec; 68°, 30 sec; 72°, 20 sec. Products were electrophoresed through a 0.8% agarose, 0.5× TBE gel. Primers for the PCR were exon 1 (forward), 5′-TCCCACAATGGCTCGTCCAGTATAGG-3′; exon 2 (reverse), 5′-AACACGCTTCAGCAGCTCGCTGTACG-3′; and *lacZ* (reverse), 5′-GCCGAGTTAACGCCATCAAAAATA-3′.

Histology: Testes histology and electron microscopy were performed as described (Ross *et al.* 1998) using Bouins-fixed material sectioned at 5 μm. X-gal staining was performed on paraformaldehyde-fixed tissues as described (MacGregor *et al.* 1995).

Behavioral analysis: *Grouped aggression in a neutral arena* was analyzed as described (Demas *et al.* 1999). *Resident-intruder aggression* was analyzed as described (Demas *et al.* 1999). Sexually experienced, gonadally intact adult B6 males from a stud colony were used as intruders. Littermates of ROSA22 homozygotes were used as controls. Bedding in the home cages was not changed for at least 3 days prior to testing. To facilitate identification of animals, intruders were marked on their tails with a nonodor pen before testing. In each trial, an intruder was placed in the home cage of a sexually experienced, singly caged homozygous ROSA22, heterozygous ROSA22, or wild-type (resident) male and the latency to attack was recorded. Tests were videotaped and lasted 20 min or until a fight occurred. Aggressive and submissive behavioral activity was noted (Grant and Mackintosh 1963) and the timing of each event was recorded. To reduce the attack latency, two rounds of testing were performed with the resident female remaining in the cage during testing. We attempted to assess the status of aggression in homozygous ROSA22 females using the postpartum aggression paradigm in which an intruder male or female is added to the home cage of a lactating nursing female (Gandelman 1972). However, no aggressive response could be elicited from the wild-type ROSA22 females on this particular genetic background.

Mating behavior: Matings of mutant and control males with superovulated B6 females were established at 5 p.m., and the presence of copulation plugs was determined between 8 and 10 a.m. the following morning. Individual males were tested on multiple occasions with 2–3 days of rest before testing with a new female. Results were analyzed using chi-square analysis.

Serum testosterone: Adult male ROSA22 (+/+, +/−, and −/−) littermates were deeply anesthetized with Avertin and blood was collected by cardiac puncture. Serum was collected in glass tubes and stored at −80° until analysis. Radioimmunoassays (RIAs) of serum testosterone levels were performed using the Biotrak testosterone/dihydrotestosterone (^{3}H) assay system (Amersham Pharmacia, Piscataway, NJ) following the protocol provided. Dilution standards, background controls, zero dose controls, and samples were all assayed in duplicate. Seminal vesicle wet weight was determined and is expressed relative to total body weight. Data for both assays of testosterone were analyzed by single-factor ANOVA.

Body mass: Mice were weighed every 3 days from postnatal day 10 through 3 months of age. Additional animals were weighed for later time points. In all instances, animals used for weight analysis were housed with same-sex littermates from weaning.

Carcass composition: Carcass composition was measured using a modification (Bartness 1987) of the method of Leshner *et al.* (1972). Data were analyzed using ANOVA (SigmaStat 2.0; Jandel Scientific Software, San Rafael, CA). Duncan's new multiple range tests were used for *post hoc* tests when appropriate. Differences among group means were considered statistically significant if $P < 0.05$.

Cloning and mapping of retroviral integration site in ROSA22: The site of retroviral integration was isolated from a homozygous ROSA22 genomic DNA library cloned in λ-DASH II (Stratagene, La Jolla, CA; Ausubel *et al.* 1994). Subclones from 12 independent phage clones were sequenced at least twice and ambiguities were resolved by sequencing

the opposite strand. Mapping was facilitated using a *Bam*HI restriction fragment length polymorphism between B6 (7.5 kb) and *Mus spretus* (9.5 kb) detected by a 4.0-kb *Not*I fragment. The Jackson Laboratory interspecific species backcross panel (C57BL/6JEi × SPRET/Ei)F_1 × SPRET/Ei (Jackson BSS) was used as described (Rowe *et al.* 1994). Raw data are available at http://www.jax.org/resources/documents/cmdata/bkmap/BSS10data.html.

RT-PCR analysis of expression of wild-type and mutant alleles: Total testis RNA (4 μg) was reverse transcribed using primers specific for *Gtrgeo22* and *lacZ*. Twenty-microliter reactions contained 0.5 units RNAGuard (Amersham Pharmacia) and 20 units SuperScript II MoMLV reverse transcriptase (Life Technologies, Rockville, MD) in the buffer supplied with the enzyme. Reactions were incubated at 95° for 2 min prior to addition of reverse transcriptase (RT) and then at 37° for 30 min and 95° for 5 min to inactivate the RT. Primers for the RT reactions were *Gtrgeo22*, 5′-GCTTGACCTTGGCAATGAAGAGGG-3′ and *lacZ*, 5′-GCCGAGTTAACGCCATCAAAAATA-3′. One-half percent of the total reverse transcription reaction was used in a three-primer PCR containing each primer (500 nM), dNTPs (500 μM), and AmpliTaq polymerase (Perkin-Elmer, Boston) in AmpliTaq buffer. Reaction conditions were 35 cycles of 95°, 45 sec; 68°, 30 sec; 72°, 20 sec. Primers for the PCR reaction were exon 1 (forward), 5′-GGCACCTTCGCCTGGCTCACCA-3′; exon 2 (reverse), 5′-AACACGCTTCAGCAGCTCGCTGTACG-3′; and *lacZ* (reverse), 5′-CCGTGCATCTGCCAGTTTGAGGGGA-3′.

Screening of cDNA library: A 2-week-old mouse brain cDNA library was generously provided by J. Chamberlain (University of Washington). The library was screened using a 550-bp DNA probe from near the retroviral integration site, which was predicted to contain exonic sequence based on high homology with the human genomic DNA. Of 70 positive clones isolated, 22 were analyzed by PCR to determine the size of the cDNA insert. PCR primers were forward, 5′-TACCACTACAATGGATGATG-3′, and reverse, 5′-GATGCACAGTTGAAGTGAAC-3′. A total of 14 reactions produced distinct cDNA products of which 7 were selected for sequencing. cDNA sequencing was performed on an ABI 373A sequencer using ABI PRISM Dye Terminators (Perkin-Elmer).

Computer-based sequence analysis: Analysis of the *Gtrgeo22* cDNA and the predicted GTRGEO22 amino acid sequence was performed using several algorithms. Comparison of *Gtrgeo22* to database sequences was performed using the BLAST algorithm (http://www.ncbi.nlm.nih.gov/BLAST/). Potential transmembrane domains were identified using the TMPred program (http://www.ch.embnet.org/software/TMPRED_form.html; Hofmann and Stoffel 1993) and the PHD program at the PredictProtein internet site (http://www.embl-heidelberg.de/predictprotein/; Rost 1996) in addition to a Kyte-Doolittle analysis. The human ortholog *GTRGEO22* is contained within clones with GenBank accession nos. AC005775 and AC011531.

Northern analysis: Total RNA was isolated by guanidium thiocyanate extraction and Northern blot analysis was performed following standard protocols (Ausubel *et al.* 1994). Polyadenylylated mRNA was purified from total RNA with the PolyATract mRNA isolation system (Promega). A 1.3-kb *Gtrgeo22* cDNA restriction fragment (*Kpn*I) and the *Bsg* control probe were labeled with [α-^{32}P]dCTP. The blot was hybridized using standard conditions, washed to 0.1× SSC, 0.1% SDS at 65°, and exposed for 14 days to Kodak BioMax MS film with an intensifying screen. Following autoradiography, membranes were rehybridized with an 18S rRNA control probe.

Ribonuclease protection assay (RPA): The regions of genomic DNA from *Gtrgeo22*, *Madcam1*, and *Cdc34* that were used to generate riboprobes each consisted of a contiguous region of genomic DNA containing transcribed and untranscribed DNA sequence. The specific sequences used are available upon request. [^{32}P]UTP-labeled riboprobes were produced using linearized plasmid templates in conjunction with an *in vitro* transcription kit (Ambion, Austin, TX) as instructed by the manufacturer. RPA was performed using a RPA II kit (Ambion) as described by the manufacturer. Twenty micrograms of total RNA were hybridized overnight to denatured antisense riboprobes at 42°. RNase digestion was performed using 2.5 units/ml RNAseA and 100 units/ml of RNAse T1 for 30 min at 37°. Reaction products were resolved by denaturing polyacrylamide gel electrophoresis. After drying down, the gel was imaged and signals quantified following exposure to a phosphoimager screen (ImageQuant, Molecular Dynamics, Sunnyvale, CA).

RNA *in situ* hybridization: The distribution of *Gtrgeo22* mRNA was determined with *in situ* hybridization using two ^{35}S-labeled, 40-bp antisense oligonucleotide probes corresponding to bases 1489–1528 and 1549–1588 of the *Gtrgeo22* mRNA. Freshly frozen brains were sectioned at 20 μm, thaw mounted on Superfrost/Plus slides (Fisher), and stored at −80° until use. *In situ* hybridization was performed as previously described (Wang *et al.* 2000). Following the *in situ* hybridization, slides were exposed to Kodak BioMax MR film for 7 weeks. The two probes used were 5′-CAGTTTGCAGGTCCCAAGTCCTGGGCAGGTGGCGGGATGT-3′ and 5′-TGCAAAGTCCAAGCGGGTACCCCTTCCTGGGTGATGACCC-3′.

RESULTS

Homozygous ROSA22 males are sterile: ROSA22 mice were generated by insertional mutagenesis using the ROSAβ-geo gene-trap retrovirus (Friedrich and Soriano 1991). Intercross of ROSA22 heterozygotes generated offspring with a ratio of 75 +/+, 180 +/−, and 72 −/−. This is not significantly different from a 1:2:1 Mendelian ratio ($\chi^2 = 3.39$, $P = 0.18$, 2 d.f.), indicating that embryonic and early postnatal development of ROSA22 homozygotes on this C57BL/6, 129S4 hybrid genetic background are unaffected by the mutation. No difference was observed in litter sizes obtained from matings of either homozygous or heterozygous ROSA22 females with wild-type or heterozygous males (data not shown). However, homozygous ROSA22 males failed to sire offspring after being paired with females. This did not result from failure in mating behavior as no significant difference was observed in the frequency of mating when homozygous ROSA22 males were compared with control littermates (copulation plugs: 13/24 for +/+, 27/48 for +/−, and 19/48 for −/− ROSA22 males; $P = 0.47$ with $n = 8$ +/+, 11 +/−, 16 −/− animals). In addition, no obvious difference was detected in mating behavior of homozygote males compared to that of controls following introduction of a female into the male's home cage, using criteria including latency to investigation of female, frequency of anal-genital sniff, and latency to mounting (data not shown). Spermatogenesis in homozygous and control ROSA22 animals was analyzed by histology (Figure 1).

Spermatozoa with normal morphology were observed in the epididymis from wild-type and heterozygous RO-

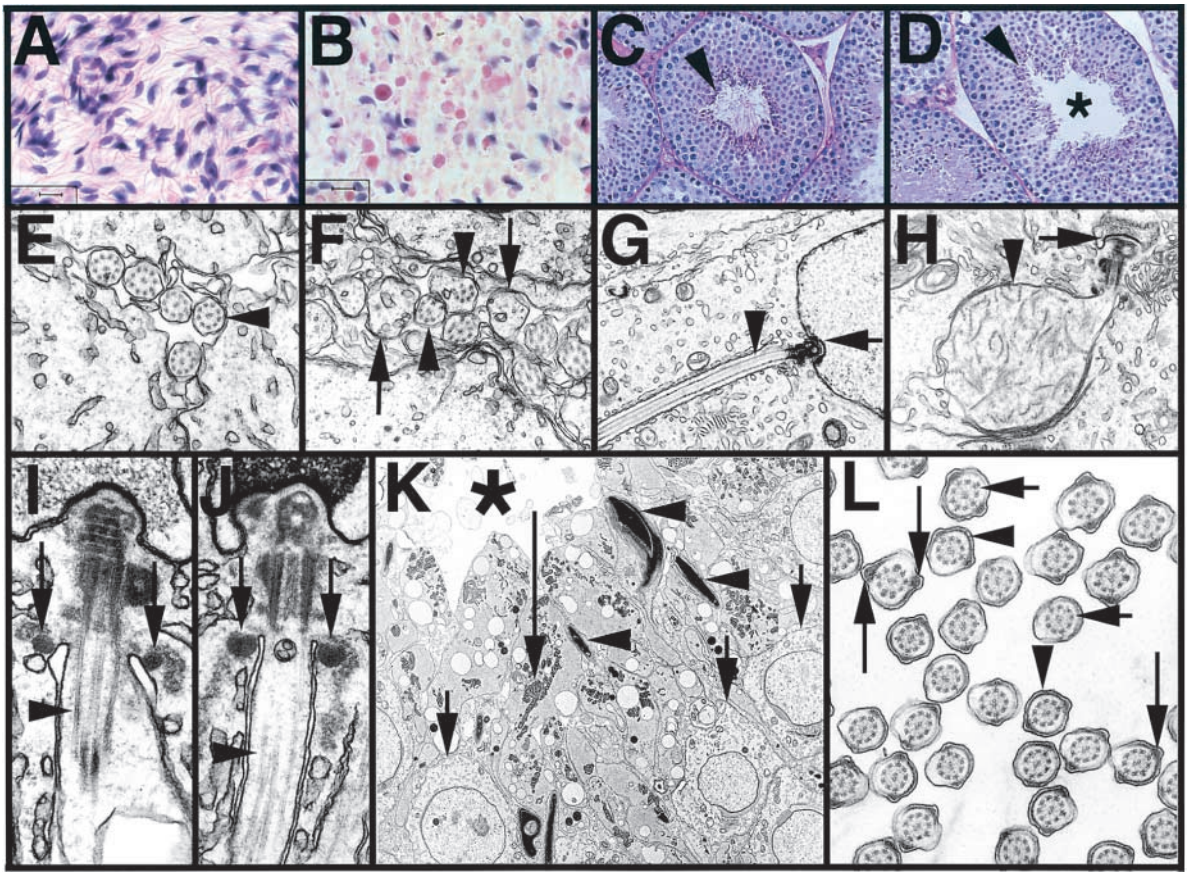

FIGURE 1.—Light and electron microscopy of spermatogenesis in ROSA22 mice. (A) Morphology of epididymal spermatozoa in wild-type animal. No difference between spermatozoa in wild-type animals compared to that in ROSA22 heterozygotes was observed (×1000). (B) Morphology of epididymal spermatozoa in ROSA22 homozygote. Spermatozoon head morphology appears grossly normal. However, spermatozoa in ROSA22 homozygotes lack flagella (×1000). (C) Histology of seminiferous epithelium in a phenotypically normal ROSA22 heterozygote animal at stage VII of spermatogenesis. Heads of elongate spermatids are located at the apical aspect of the Sertoli cell (arrowhead) with their flagella projecting into the lumen (×200). (D) Stage VII spermatogenesis in a ROSA22 homozygote. Spermatid heads (arrowhead) have a similar location; however, no flagella are present in the tubular lumen (asterisk; ×200). (E) Transverse section of primary axonemes (*e.g.*, arrowhead) in step 1 spermatids from a ROSA22 homozygote. The "9 + 2" axonemal structure appears grossly normal (×35,000). (F) Transverse section of primary axonemes in step-2–3 spermatids from a ROSA22 homozygote. Axonemes lack microtubule outer-doublet pairs (arrowheads) or are severely disorganized (arrows; ×35,000). (G) Longitudinal section of primary flagellum in step-9 spermatid from wild-type control. The central pair and outer microtubules of the axoneme appear normal (arrowhead). The implantation fossa is indicated (arrow). Only the proximal portion of the developing flagellum is shown (×10,000). (H) Longitudinal section of flagellum in step-10 spermatid from a ROSA22 homozygote. The flagellum (arrowhead) is greatly truncated and contains what, on the basis of diameter and size, appear to be fragmented microtubules (×16,000). (I) Longitudinal section of proximal flagellum in step-13 spermatid from wild-type animal. The central pair and outer microtubules (arrowhead) of the axoneme appear organized. The annulus (arrows) is indicated (×40,000). (J) Longitudinal section of primary flagellum in step-13 spermatid from ROSA22 homozygote. The axoneme appears abnormal with bent and poorly organized microtubules (arrowhead). The annulus (arrows) is still present at this stage (×40,000). (K) Stage VII seminiferous epithelium in homozygous mutant containing elongate step-16 (arrowheads) and step-7 (short arrows) round spermatids. Mature flagella are absent from the lumen of the tubule (asterisk). The cytoplasm of step-16 spermatids contains structures resembling outer dense fibers (long arrow; ×400). (L) Cross section through distal flagellum of mature step-16 spermatids in wild-type animal. The axoneme (short arrows) is surrounded by the longitudinal columns (long arrows) and transverse ribs (arrowheads) of the fibrous sheath (×35,000).

SA22 animals (Figure 1A). In contrast, epididymal spermatozoa in ROSA22 homozygotes lacked flagella (Figure 1B). Examination of testis histology revealed that the defect in flagellar formation arose prior to spermiation of elongate spermatids (Figure 1, C and D). To identify the nature of the defect in flagellar development, haploid male germ cell development in ROSA22 homozygotes was examined using electron microscopy (EM). In mutants, the structure of the axoneme in step 1 spermatids appeared grossly normal (Figure 1E). However, beginning at steps 2–3, approximately one-half of the flagellar cross sections displayed abnormalities that ranged from absence of outer or central microtubule doublet pairs to complete disorganization of the axonemal complex (Figure 1F). No defect was detected in the relocation of the paired centrioles to abut the nu-

clear membrane or in the initial formation of the annulus. By step 5, almost all flagella displayed abnormal development and intact axonemes were rarely observed. By steps 9–11, remnants of the flagellum were in a highly contracted state and contained disorganized microtubule-related structures (Figure 1H). In spermatids containing a truncated axoneme at this stage, the structure was abnormal with bent microtubules and apparently poor connection to the distal centriole (Figure 1J). Late in spermiogenesis (steps 12–16) the contracted flagellar structure had detached from the head (Figure 1K). Shortly before spermiation, structures resembling ODFs that were not associated with the flagellum were observed in the cytoplasm (Figure 1K). Axonemes of mature spermatids in control animals appeared normal (Figure 1L). At spermiation, heads were released in an apparently normal manner in ROSA22 homozygotes. No evidence was found for defects in mitosis or meiosis of male germ cells (data not shown).

Absence of intermale aggression: It was noted that homozygous ROSA22 males failed to attack each other when caged together. Consequently, intermale aggressive behavior was analyzed using a resident-intruder experimental paradigm (Demas *et al.* 1999). All wild-type ($n = 6$) and heterozygous ROSA22 ($n = 7$) resident males analyzed attacked a gonadally intact C57BL/6 (B6) intruder within a 20-min period. In contrast, no ROSA22 homozygote resident male ($n = 9$) attacked the B6 intruder or displayed aggressive postures, such as chasing, lunging, aggressive grooming, biting, mounting, tail-rattling, or attacking (Grant and Mackintosh 1963). Moreover, in 7 out of 26 trials the intruder eventually attacked the resident within the 20-min test period. When attacked by an intruder, ROSA22 mutant males would assume an upright defensive posture (Grant and Mackintosh 1963) and would attempt to retreat, but would never respond with aggressive behavior. ROSA22 homozygote males are smaller than control male littermates (Figure 2B). To determine if animal size influenced the lack of intermale aggression, we examined this behavior using a grouped aggression in a neutral arena (grouped housing) paradigm (Demas *et al.* 1999). Wild-type or heterozygous ROSA22, sexually experienced males that had previously been individually caged invariably elicited an aggressive response with a latency of a few minutes. Remarkably, despite grouped housing for >24 hr of 10 similarly sized, sexually experienced ROSA22 homozygote males, no aggressive attacks or posturing was observed.

Both normal sexual development and the overtly normal mating behavior of homozygous ROSA22 males suggested that levels of circulating testosterone (T) were unaffected. To test this, steady-state levels of T were quantified using two independent methods, RIA of serum T and weight of paired seminal vesicles from adults. As expected from the pulsatile nature of release of T, significant fluctuation was observed in the level of circulating T in animals from each genotype group, with no significant difference being observed between the three groups (+/+, average 3.3 ng/ml serum, SE 4.8, range 0.14–12.11, $n = 10$; +/−, average 2.0 ng/ml serum, SE 3.1, range 0.35–6.65, $n = 4$; −/−, average 1.9 ng/ml serum, SE 3.1, range 0.21–10.0, $n = 11$, single factor ANOVA $P = 0.72$). Comparison of wet weight of seminal vesicles is a reliable indicator of relative levels of circulating testosterone in mice (Barkley and Goldman 1977; Van Oortmerssen *et al.* 1987). No significant difference was observed in the weights of adult paired seminal vesicles between the different genotype classes (+/+, 8.9 mg/g, ±1.5, $n = 5$; +/−, 9.4 mg/g, ±2.4, $n = 6$; −/−, 9.6 mg/g, ±2.0, $n = 11$; expressed as milligrams paired seminal vesicle weight per gram of body mass, single factor ANOVA $P = 0.83$). Together, these data indicate no significant difference in the level of circulating T in ROSA22 homozygotes compared to that in control animals.

To assess general olfactory function, ROSA22 homozygote and control males, which had been fasted overnight, were placed individually into a clean rat cage containing fresh bedding and the time to locate a piece of chocolate hidden 1 cm beneath the bedding was recorded. No difference was found in the latency to locate the chocolate between the different groups of animals ($n = 5$ of each genotype).

Reduced body fat content in adult male ROSA22 homozygotes: Adult ROSA22 homozygotes are smaller than their control littermates (Figure 2, A and B). To determine when the reduction in body mass of ROSA22 mice is first observed, cohorts of littermates were weighed with a 3-day interval from postnatal day 10 (P10) until 3 months of age and intermittently thereafter. A clear difference in the body mass of ROSA22 homozygotes compared to that of control littermates was first observed in postpubertal animals (Figure 2B). No significant difference was found in daily food consumption or resting body temperature of mutant and control animals (data not shown), suggesting that the reduced body mass did not result from either hypophagia or increased resting metabolic rate. Similarly, preparation of skeletons from adult ROSA22 homozygotes revealed no obvious difference in skeletal size compared to littermates (data not shown). To determine if the reduced body mass was associated with altered body composition, percentage of water, lipid, and fat-free dry mass was measured for each animal in cohorts of age-matched male and female mutant and control ROSA22 littermates between 10 and 17 months of age. The reduced weight in male homozygotes was associated with a significant reduction in body fat content ($P < 0.01$; Figure 2C). Reduction in fat content of female homozygotes was a trend and was not significant at $P < 0.05$.

Mutated gene is expressed at low steady-state levels in several tissues: To determine where the mutated gene was transcribed, expression of the β-geo gene-trap prod-

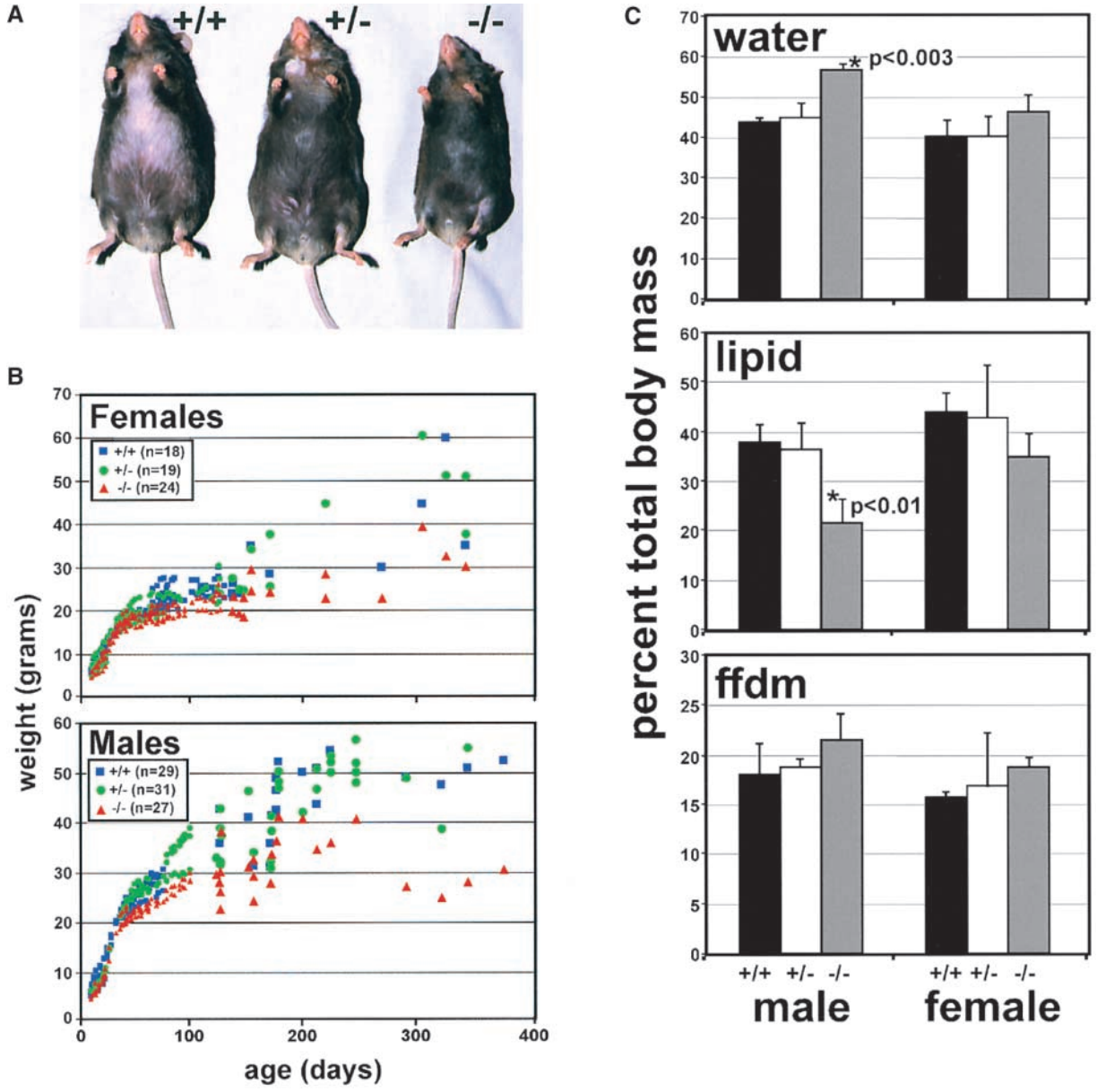

FIGURE 2.—Reduced body fat mass in adult ROSA22 homozygous mice. (A) Wild-type (49.1 g), heterozygous mutant (49.2 g), and homozygous mutant (27.2 g) male ROSA22 animals at 9 months of age. (B) Body mass for multiple cohorts of ROSA22 animals. Weights are plotted for mutant and control littermates between postnatal day 10 and over 12 months of age. For any single time point, mutant and control littermates are vertically aligned. The data set for the larger symbols (animals over ~100 days of age) is derived from 17 +/+, 25 +/−, and 20 −/− males and 9 +/+, 12 +/−, and 15 −/− females. Homozygous ROSA22 mice weigh less than their control littermates at all ages analyzed. (C) Analysis of body composition in ROSA22 animals. Homozygous ROSA22 males have a significant ($P < 0.01$) reduction in body lipid content and corresponding relative increase in water and fat-free dry mass (ffdm). Homozygous ROSA22 females also have reduced lipid content, although this was a trend only in the animals sampled. The data are derived from analysis of five cohorts of mutant and control littermates, composed of 3 +/+, 2 +/−, and 3 −/− males and 2 +/+, 3 +/−, and 3 −/− females, all between 10 and 17 months of age.

uct was analyzed using X-gal histochemistry. In all tissues, significant β-geo activity could be detected only following overnight incubation at 37°, suggesting that the mutated gene was expressed at low levels. As anticipated from the male sterility phenotype, β-geo activity was observed in seminiferous epithelium, where it was localized to both Sertoli cells and germ cells (Figure 3A). β-geo activity was also observed in olfactory epithelium, lung, trachea, proximal oviduct, and the vomeronasal organ (VNO; Figure 3, B–F), with expression of the β-geo reporter gene being restricted to the ciliated epithelium. The mutated gene was also expressed in the central nervous system (CNS) including the cerebral cortex, habenula, amygdala, paraventricular nucleus (PVN) and ventromedial nucleus of the hypothalamus (VMH), lateral olfactory tract nucleus (LOT 2), and hippocam-

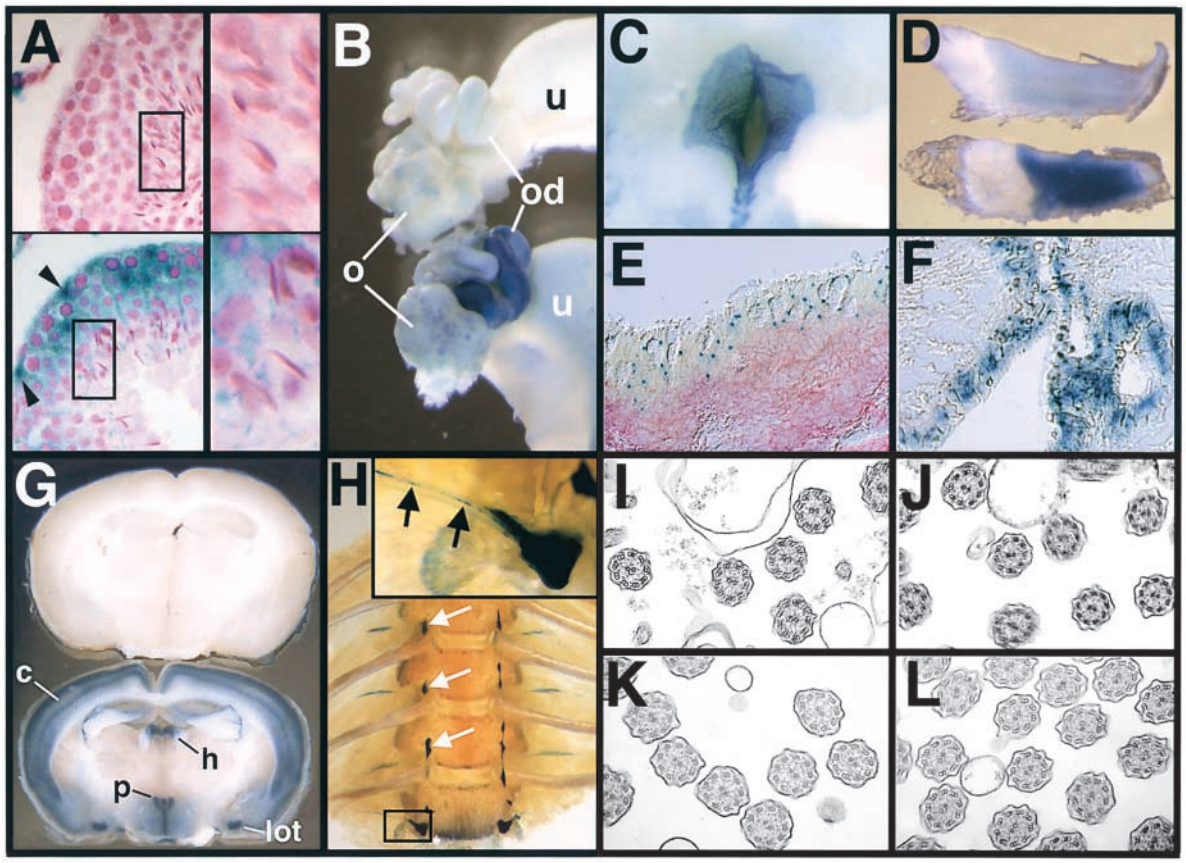

Figure 3.—Expression of the mutant allele of *Gtrgeo22* in ROSA22 mice. Expression of the mutant allele was examined by X-gal staining of fixed tissue from ROSA22 homozygote and control mice. Blue staining indicates expression of the mutant allele. (A) Seminiferous epithelium from wild type (top) and ROSA22 homozygote (bottom). β-geo activity is seen in Sertoli cells (arrowheads) as well as in all stages of developing germ cells, including round and elongating spermatids (×200; ×500 insets). (B) Proximal oviduct: wild type (top) and mutant (bottom; ×15). (C) Ependymal layer of third ventricle in CNS (×15). (D) Vomeronasal organ: wild type (top) and ROSA22 homozygote (bottom; ×15). (E) Olfactory epithelium (×400). (F) Bronchial epithelium (×400). (G) Midcoronal section of CNS from wild type (top) and homozygote (bottom; ×5). (H) Sympathetic chain ganglia of autonomic system (white arrows) and axon tracts (black arrows) from dorsal root ganglia (×5; ×25 inset). (I–L) EM of transverse section of ciliary axoneme in oviduct from wild type (I) and homozygous mutant (J) or trachea from wild type (K) and homozygous mutant (L) (I–L ×50,000). c, cerebral cortex; h, habenula; o, ovary; od, proximal oviduct; lot, second nucleus of the lateral olfactory tract (LOT2); p, PVN; u, uterus.

pus (Figure 3G) as well as within the ependymal layer lining the ventricles (Figure 3C). No expression was detected within the striatum or cerebellum and no sex-specific pattern of expression was observed (data not shown). Expression of the mutant allele was also detected within the sympathetic nervous system (Figure 3H). The grossly normal development of ROSA22 homozygote mice suggested that axonemal structure was unlikely to be affected in all tissues. Indeed, analysis of axonemes in ciliated epithelia from ROSA22 homozygotes by EM failed to show abnormalities similar to those observed in spermatids Figure 3, I–L).

Molecular genetic analysis of the gene mutated in ROSA22 mice: The site of retroviral integration was mapped to chromosome 10. To identify expressed sequences, ~16 kb of genomic DNA flanking the proviral integration site was sequenced and compared to genetic databases (Altschul *et al.* 1990). Comparative genomic sequence analysis was used to identify exons for the mutated gene on the basis of its conservation with the orthologous region of the human genome. The results were used to generate a probe that was predicted to represent a portion of an exon and this was used to screen a mouse brain cDNA library. Several independent cDNAs were isolated and sequenced. The coding sequence of *Gtrgeo22* cDNA and the human ortholog is shown in Figure 4A. The *Gtrgeo22* cDNA contains one large and several small open reading frames (ORFs). In the human sequence, the large ORF is highly conserved while the smaller ones are not. This suggests that the large ORF encodes the polypeptide that is mutated in ROSA22 mice. Comparison of the cDNA and genomic DNA sequences revealed that both the human and mouse GTRGEO22 coding sequence are contained within two exons that share identical exon-intron boundaries (Figure 4B). Reverse transcriptase-PCR (RT-PCR) analy-

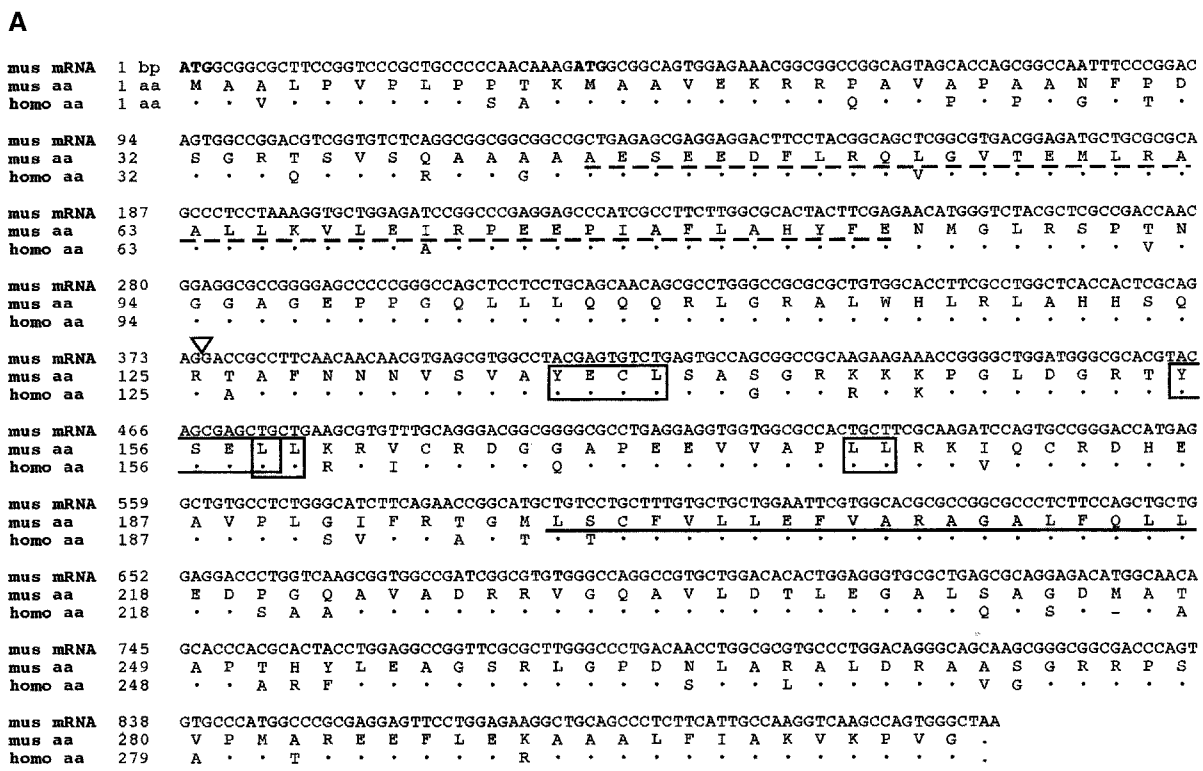

FIGURE 4.—Identification of the gene mutated in ROSA22 mice. (A) *Gtrgeo22* cDNA open reading frame is shown with the mouse and human predicted peptide sequence below. The single conserved ORF is 909 nucleotides with a 5′ untranslated region (UTR) of 473 bp and a 194-bp 3′ UTR. In both humans and mice, the ORF has two in-frame alternative initiator methionine codons located 36 bp apart (boldface type), each of which has similar homology to the Kozak consensus sequence for eukaryotic translation initiation (KOZAK 1987). The amino acid sequence for the human ortholog is identical except where indicated. The region with limited homology to the dimerization domain of RIα subunit of protein kinase A is underlined with a dashed line. Canonical dileucine and YXXØ motifs are boxed. The open arrowhead indicates the position of the intron and the predicted transmembrane domain in exon 2 is underlined (Kyte-Doolittle hydropathy plot score 1.71; window 19, cut-off threshold for significance >1.58). The human consensus cDNA sequence has a 3-bp deletion that removes a methionine at position 246. The human ortholog of *Gtrgeo22* is contained within clones with GenBank accession numbers AC005775 and AC011531. (B) Genomic organization of *Gtrgeo22* and the human ortholog *GTRGEO22*. *Gtrgeo22* is encoded by two exons in both mice and humans. In ROSA22 mice, the ROSAβ-geo provirus integrated within the single intron of *Gtrgeo22*. The putative transcriptional start site for *Gtrgeo22* transcripts is ~400 bp downstream of the polyadenylylation signal for *Madcam1*. *Cdc34*, which encodes an ubiquitin conjugating enzyme is located ~6 kb downstream of *Gtrgeo22*. The gene order and orientation is maintained in humans. *GZMM*, *GRANZYME M*; *BSG*, *BASIGIN*. (C) RT-PCR analysis of transcripts from wild-type and mutant *Gtrgeo22* alleles. The graphic indicates the position of the primers used for RT (c and y) and amplification of transcripts from the wild-type (a and b) or mutant (a and x) alleles, as well as the predicted size of the amplification products. The photograph on the right illustrates the result of the RT-PCR using testis RNA from wild-type (+/+), homozygote (−/−), and heterozygote (+/−) ROSA22 mice. The absence of a 143-bp product in the sample from the homozygote mutant indicates no significant level of wild-type transcript in homozygous mutant testes. Analysis of brain RNA produced essentially similar results (data not shown).

sis confirmed that the provirus trapped *Gtrgeo22* transcription *in vivo* (Figure 4C). Moreover, no wild-type mRNA was detected in total RNA extracted from the testis of a ROSA22 homozygote (Figure 4C). It is possible that the existing mutant allele of *Gtrgeo22* may not be a functional null. However, the mutant gene product lacks the predicted transmembrane domain and the allele does not appear to be hypomorphic for the wild-type product.

DNA sequence analysis revealed that *Gtrgeo22* is closely flanked by two previously identified genes, *Madcam1* (BRISKIN *et al.* 1993) and *Cdc34* (PLON *et al.* 1993; Figure 4B). Previous studies demonstrated that mutation of a locus by integration of a mini-gene can perturb the expression of neighboring genes (OLSON *et al.* 1996). To determine whether the phenotypes observed in ROSA22 homozygotes could have resulted from deregulated expression of *Madcam1* and *Cdc34*, steady-state levels of mRNA for these genes were quantified in tissues from mutant and control ROSA22 animals using ribonuclease protection assay and the results were normalized to expression of β-actin (Figure 5A). No difference was noted in the relative amount of *Madcam1* RNA in spleens from control or mutant ROSA22 animals (Figure 5A). Similarly, no difference was observed in levels of expression of *Cdc34* in either brain or testis of control and mutant animals (Figure 5A). Consequently, the phenotypes observed most likely arise from mutation of *Gtrgeo22*.

The longest mouse *Gtrgeo22* cDNA isolated was 1579

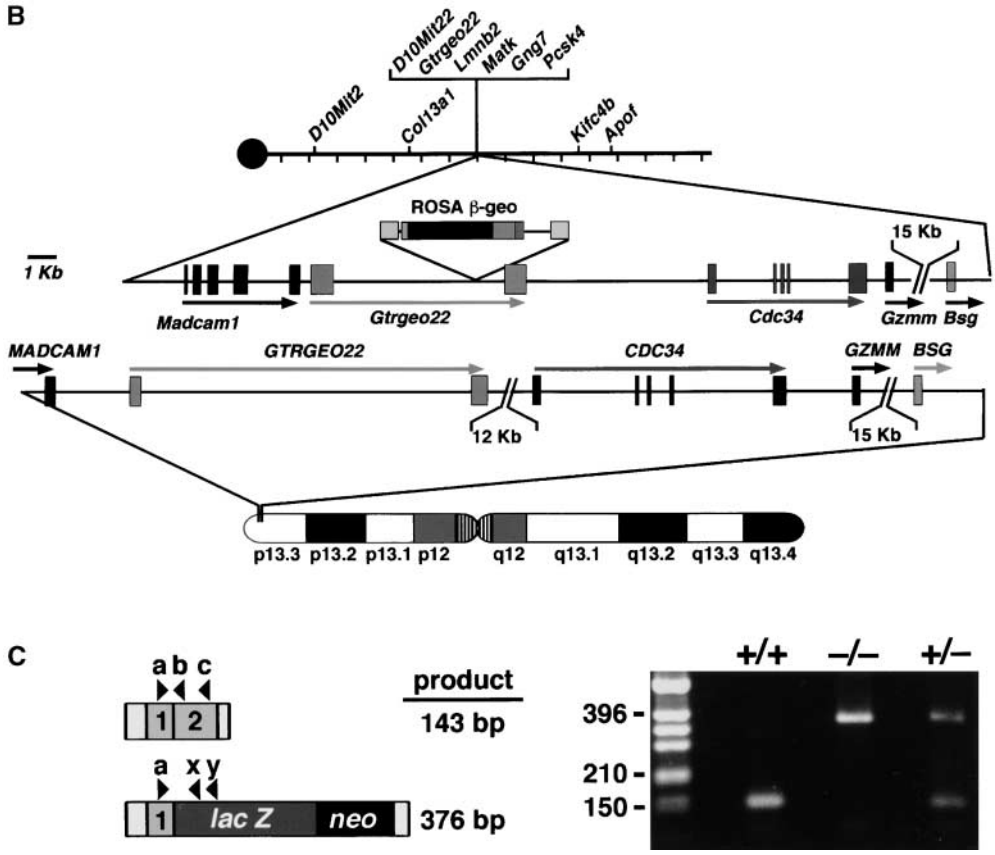

FIGURE 4.—*Continued.*

bp. Northern analysis of testis RNA isolated from mutant and control littermates indicates that this is consistent with a full-length transcript (Figure 6A). The results of the Northern analysis are consistent with the RT-PCR analysis, which suggests that no mRNA is present in testis that could encode the wild-type gene product. In wild-type mice, the timing of the first wave of spermatogenesis has been defined, with haploid spermatids first appearing between P20 and P22 (NEBEL *et al.* 1961). An increase in the overall steady-state level of *Gtrgeo22* transcripts in testis was observed at P22 (Figure 6B), which is consistent with a role of *Gtrgeo22* in the early stages of spermatid flagellar development. However, as suggested by the pattern of β-geo activity observed in the testis of ROSA22 homozygotes, *Gtrgeo22* is also expressed in testis during the first wave of male gametogenesis, prior to development of haploid germ cells.

Correlation of β-geo activity with transcription of wild-type allele: Staining of tissues from ROSA22 homozygotes suggested that the wild-type allele was expressed at low levels in a wide range of tissues. Consistent with results of the histochemical analysis, Northern analysis also revealed relatively low steady-state levels of *Gtrgeo22* transcripts in tissues that stained with X-gal, including oviduct, brain, and testis (Figure 6C). Transcripts were also observed in several other tissues including heart, kidney, and liver, although these tissues did not stain uniformly with X-gal. It is possible that the mRNA expression observed in these latter tissues originates in the peripheral nervous system (PNS), as X-gal staining was observed within the autonomic nervous system at sites of innervation of heart and adrenals, as well as in the paravertebral sympathetic chain ganglia (Figure 3H and data not shown).

To determine if expression of β-geo from the mutant allele was representative of the pattern of expression of the cognate, wild-type gene at the cellular level, the X-gal expression pattern in the CNS was compared with RNA *in situ* hybridization. With the exception of the granule layer of the dentate gyrus, the pattern of β-geo expression within the CNS accurately reflects the pattern of transcription of the wild-type gene (Figure 7, A–C). Expression within the CNS appeared to be neuronal, *e.g.*, in pyramidal cells in the cerebral cortex (Figure 7D).

***Gtrgeo22* encodes a novel transmembrane protein containing dileucine and tyrosine (YXX∅) motifs:** Analysis of the cDNA sequence with several computer algorithms suggests that *Gtrgeo22* encodes a novel 303-amino-acid single-pass type II transmembrane (TM) protein of ~34 kD, with a cytoplasmic tail of amino acid residues 1–191. The predicted TM domain is contained within exon 2, which is not transcribed in the existing mutant allele (Figure 4A). Comparison of the peptide sequence with multiple databases failed to reveal any significant homology to previously identified polypeptides, with the exception of limited homology to the dimerization domain of the RIα regulatory subunit of protein kinase A

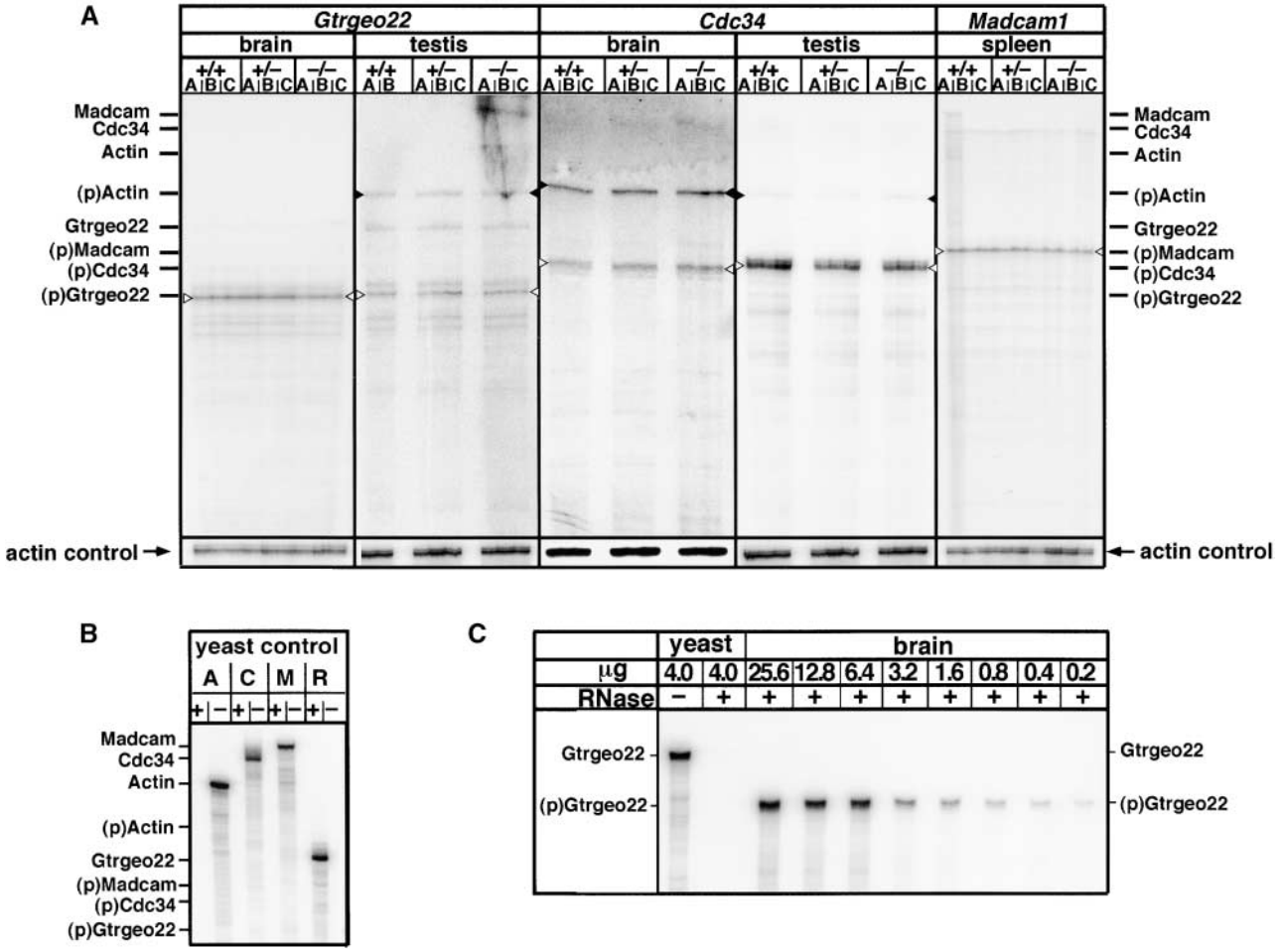

FIGURE 5.— RPA of *Gtrgeo22*, *Madcam1*, and *Cdc34* expression in ROSA22 mice. (A) RNA was isolated from brain, spleen, and testis from three cohorts (A–C), each composed of three littermates (one each of +/+, +/−, −/−). The expected size of the unprotected and protected (p) products is shown for each riboprobe. For each assay, a control reaction was performed using a β-actin probe and this was used to normalize the signal from the experimental probe. In some cases the actin probe was combined with the experimental probe. The *Gtrgeo22* riboprobe is derived from the first exon, which is transcribed in the mutant allele. (B) Negative controls to verify specificity of protection. Full-length riboprobes were hybridized with yeast t-RNA and reacted with (+) or without (−) RNAse A. (C) To verify that the RPA could accurately quantify mRNA, twofold dilutions of brain RNA from a wild-type mouse were prepared and steady-state levels of *Gtrgeo22* mRNA were analyzed using a phosphoimager. The values of the protected probe (p) were in a linear range (data not shown).

(Figure 4A). Examination of expressed sequence tag databases revealed that orthologs of *Gtrgeo22* exist in Xenopus and Danio, although apparently not in Drosophila or Caenorhabditis (data not shown). Inspection of the peptide sequence revealed the presence of canonical dileucine and YXX∅ (where ∅ is a bulky hydrophobic amino acid) motifs (HEILKER *et al.* 1999) in the predicted cytoplasmic side of the molecule close to the TM domain (Figure 5A). Interestingly, these motifs were also conserved in the GTRGEO22 orthologs in Danio and Xenopus. In this location, such motifs can mediate intracellular sorting of transmembrane proteins via interaction with adapter proteins and clathrin (HEILKER *et al.* 1999).

DISCUSSION

Abnormal spermatid flagellar development in ROSA22 mutants: Several mutations have been described that affect development of the spermatid flagellum in mice (HANDEL 1987; CEBRA-THOMAS and SILVER 1991). These range in severity from relatively subtle abnormalities involving an absence of specific outer microtubule doublets, *e.g.*, in VDAC3-deficient (SAMPSON *et al.* 2001) and *wobbler* (LEESTMA and SEPSENWOL 1980) mutant mice, to the complete loss of flagellar structure observed in mature spermatozoa from *Hst-6*^{s} homozygote mice (PHILLIPS *et al.* 1993; PILDER *et al.* 1993). Interestingly, there are similarities in development of the flagellar defect in ROSA22 and *Hst-6*^{s} homozygote mice. During the early stages of spermiogenesis in *Hst-6*^{s} homozygotes, the axoneme also fails to form properly, with microtubules missing or bent (PHILLIPS *et al.* 1993). By midspermiogenesis in *Hst-6*^{s} homozygotes, no axoneme can be observed, but instead, there is a "plasmalemmal balloon" filled with tubulin aggregates, similar to that seen in ROSA22 homozygotes (PHILLIPS *et al.* 1993). A

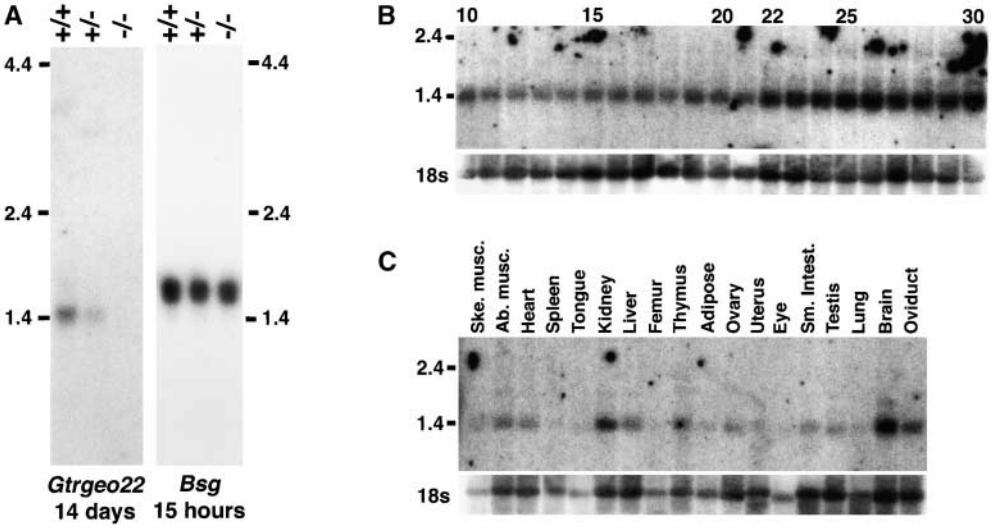

FIGURE 6.—Northern analyses of *Gtrgeo22* expression. (A) Analysis of expression of *Gtrgeo22* and *Basigin* (*Bsg*) in testis of ROSA22 mice. The Northern blot on the left [10 μg of poly(A)$^+$ RNA per lane] was probed with an exon-2 specific *Gtrgeo22* DNA sequence, which is not transcribed in the mutant allele (14-day exposure). As a control for integrity of the total RNA from which the poly(A)$^+$ was purified, the blot on the right (same gel, 10 μg total RNA per lane) was probed with a cDNA for mouse *Bsg*, which encodes a component of the sperm flagellum and which is located ~25 kb distal to *Gtrgeo22* (15-hr exposure). Note that expression of *Bsg* appears unaffected in ROSA22 homozygotes. (B) Northern analysis of total testis RNA isolated from wild-type mice of different postnatal age. (Top) Probed with a full-length cDNA to *Gtrgeo22* (14-day exposure). The numbers above the lanes correspond to the ages of mice analyzed (1-day increment). (Bottom) The blot was stripped and reprobed with an 18s RNA specific probe (30-min exposure, direct autoradiography). An increase in steady-state levels of *Gtrgeo22* transcripts in testis is apparent between P21 and P22. (C) Northern analysis of expression of *Gtrgeo22* in multiple mouse tissues. Highest steady-state levels of *Gtrgeo22* transcripts are detected in brain, kidney, and oviduct (top, 14-day exposure; bottom, 30-min exposure).

subtle difference between these two mutations is that released spermatozoa heads in *Hst-6^s* homozygotes retain a short posterior "bag" that substitutes for a sperm tail, while such a structure is not seen attached to spermatozoa heads in ROSA22 homozygotes. The genetic mutation responsible for the defective flagellar development in *Hst-6^s* homozygotes has not yet been identified. However, one strong candidate is *Dnahc8*, which encodes an axonemal dynein heavy chain (FOSSELLA *et al.* 2000).

Insight into the regulation of axonemal stability has been derived from genetic analyses in Chlamydomonas (HUANG *et al.* 1982; DUTCHER 1995; MITCHELL 2000). In Chlamydomonas, a series of flagellar (*fla*) and stumpy flagella (*stf*) mutations have been described in which instability of the algae's paired flagella is associated with disorganization or truncation of the axoneme (KOZMINSKI *et al.* 1995; COLE *et al.* 1998; PAZOUR *et al.* 1998, 1999; PORTER *et al.* 1999). Gene products affected in *fla* and *stf* mutants include kinesins and cytoplasmic dyneins that mediate intraflagellar transport (IFT) of proteins required for assembly and maintenance of the flagellum (ROSENBAUM *et al.* 1999). In mice, it is unclear how an axonemal dynein such as DNAHC8 might be required for axonemal stability in the developing spermatid flagellum via IFT of proteins. However, it has been postulated that alternate splicing of the *Dnahc8* transcripts could generate a bifunctional dynein that has both cytoplasmic and axonemal activity (FOSSELLA *et al.* 2000; PILDER and SAMANT 2001).

In contrast, GTRGEO22 does not appear to be a motor protein, although the function of GTRGEO22 in mediating flagellar axoneme assembly or stability might be involved in some manner with dyneins or kinesins. The timing of onset of the defect in flagellar development in the ROSA22 mutant could reflect either abnormal assembly of the axoneme or maintenance thereof, possibly associated with failure in subsequent assembly of the accessory flagellar structures (*e.g.*, the longitudinal columns of the FS).

Absence of intermale aggressive behavior and reduced body fat in mutant males: Homozygous ROSA22 males had a striking deficit in intermale aggression. In wild-type animals this behavior is greatly reduced following removal of the testes (BEEMAN 1947), olfactory bulbs (ROWE and EDWARDS 1971), or the VNO (MARUNIAK *et al.* 1986). The mechanisms by which such treatments decrease agonistic behavior involve reduction of levels of circulating androgen or disruption of olfaction, including pheromone reception. Genetic studies in the mouse support these conclusions. For example, intermale aggression is almost completely eliminated in mice lacking either estrogen receptor α (ERα; OGAWA *et al.* 1997) or endothelial nitric oxide synthase (eNOS; DEMAS *et al.* 1999). Mutation of the ERα blocks development of male-specific behavior associated with action of aromatized androgen (OGAWA *et al.* 1997), while the mechanism of eNOS in facilitating intermale aggression appears to involve increased rates of turnover of serotonin (NELSON and CHIAVEGATTO 2001). Mice mutant for TRP2, a putative pheromone receptor expressed within the VNO (STOWERS *et al.* 2002), fail to initiate intermale aggression in response to a male pheromone stimulus. However, attack by a wild-type male can elicit an intermale aggressive behavioral response in TRP2-deficient males, indicating that TRP2 deficiency *per se* does not block the ability of a male mouse to display aggression.

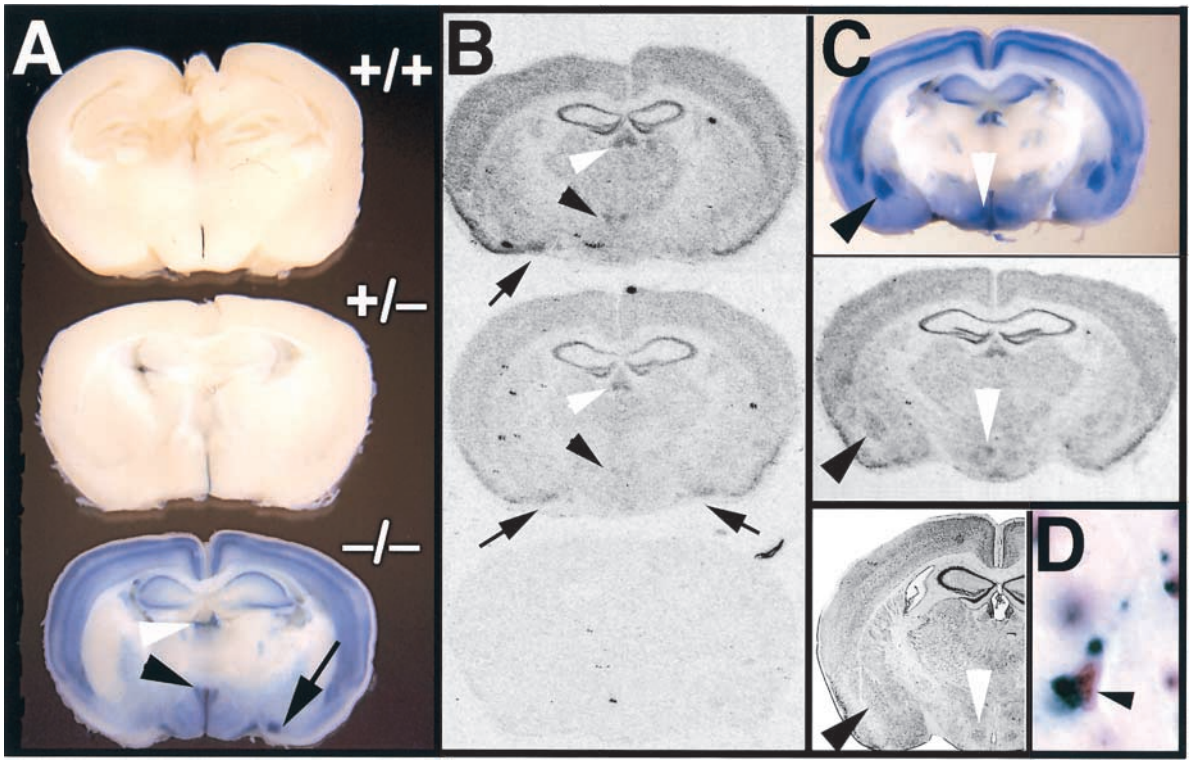

Figure 7.—Expression of the trapped gene reflects expression of the wild-type allele in most areas of the CNS. (A) Expression pattern of the mutant allele of *Gtrgeo22*, as evidenced by β-geo activity. Midcoronal 2-mm sections of brain were fixed and stained for β-geo activity using X-gal. The relatively weak X-gal staining in the section from the heterozygous animal is a reproducible finding. Biochemical analyses indicated a twofold increase in β-geo activity between heterozygous and homozygous brains; thus the dramatic difference in signals from X-gal staining is likely due to the level of β-geo activity in heterozygotes being below a threshold required to give semiquantitative histochemical staining. White arrowhead, habenula; black arrowhead, PVN; black arrow, LOT 2. (B) Expression pattern of the wild-type allele of *Gtrgeo22* in ROSA22 mice. Midcoronal sections of CNS equivalent to those in A are shown. Note the reduction in expression observed by RNA *in situ* hybridization between wild type (top), heterozygote (middle), and homozygote (bottom) ROSA22 animals. Habenula (white arrowheads), PVN (black arrowheads), and LOT 2 (black arrows) are indicated. (C) More posterior coronal sections of CNS of adult ROSA22 mice. (Top) Homozygous mutant ROSA22 brain showing expression within basolateral nucleus of the amygdala (BLA; black arrowhead) and VMH (white arrowhead). Expression is also detected at lower levels in the central and dorsolateral nuclei of the amygdala. (Middle) Approximately the same level of section from a wild-type animal analyzed by *in situ* hybridization with a *Gtrgeo22* specific probe. Expression in the BLA (black arrowhead) and VMH (white arrowhead) is indicated. (Bottom) Approximately the same level of coronal section from a C57BL/6J mouse that has been stained with Nissl to reveal regional density of cell nuclei. The BLA (black arrowhead) and VMH (white arrowhead) are indicated for the left hemisphere. Bottom of C used with permission of the publisher (Franklin and Paxinos 1997). (D) Histology of X-gal-stained cerebral cortex from homozygous ROSA22 mouse. β-geo activity is located within pyramidal cells (arrowhead; ×1000). Due to the oblique nature of some sections, the contralateral signal is often either weakly observed or not observed at all (*e.g.*, LOT 2 in bottom of A, LOT 2 in top of B, and BLA in middle of C). The only region of the CNS in which the β-geo reporter gene did not routinely appear to match the pattern of expression of *Gtrgeo22* was in the granule cell layer of the dentate gyrus.

In addition to these effects on intermale aggression, males with loss of function of either ERα or TRP2 also display abnormal male sexual behavior (Ogawa *et al.* 1997; Stowers *et al.* 2002). When compared to these mutants, the genetic defect in homozygous ROSA22 males appears novel in that in addition to a complete absence of intermale aggression, their mating behavior appeared normal. It will be of interest to determine if the mutant behavioral phenotype in ROSA22 homozygotes is epistatic to mutations that enhance intermale aggressive behavior in mice, such as that observed in neuronal NOS-deficient mice (Nelson *et al.* 1995).

A significant reduction was observed in the body fat content of adult homozygous ROSA22 males although no difference was observed in their daily food consumption or resting body temperature compared to that of control animals. These observations suggest that the reduced body fat in homozygous ROSA22 males does not result from altered resting metabolic rate or hypophagia. In light of the existing behavioral phenotype, it will be of interest to determine whether the reduced body fat results from hyperactivity. Alternatively, the altered body composition in ROSA22 mutants might arise from differences in intestinal function, where *Gtrgeo22* is also expressed.

Although *Gtrgeo22* appears to be expressed in both

germ cells and somatic Sertoli cells within the seminiferous epithelia, it seems more likely that its function in mediating flagellar development is germ cell autonomous. In contrast, it is currently less clear where expression of *Gtrgeo22* is required to facilitate intermale aggressive behavior. *Gtrgeo22* is expressed in the CNS, PNS, VNO, and olfactory epithelium and loss of GTRGEO22 function in any of these tissues theoretically could affect intermale aggressive behavior. Within the CNS, *Gtrgeo22* was expressed in the amygdala, a structure that is important for processing social and environmental cues involved in behavior (Davis 1997; LeDoux 2000). Animals in which the amygdala has been experimentally damaged display impaired response to emotional stimuli as well as altered exploratory activity (Grijalva *et al.* 1990; Davis 1997; LeDoux 2000). Although it is attractive to speculate that the absence of intermale aggression in ROSA22 mutants may be associated with defective amygdaloid or other limbic function, *a priori*, it is equally plausible that these phenotypes arise due to abnormalities in other areas of the CNS or PNS, or even in other nonneuronal tissues, that express *Gtrgeo22*. Analysis of mice lacking GTRGEO22 function specifically within the nervous system should help to clarify this issue.

How does GTRGEO22 function? *Gtrgeo22* encodes a novel gene product, which precludes immediate insight into the protein's mechanism of function. The presence of conserved dileucine and tyrosine motifs in proximity to the predicted transmembrane domain suggests that GTRGEO22 may be subject to intracellular sorting, possibly via interaction of adaptins and clathrins (Heilker *et al.* 1999). On the basis of the extremely low steady-state level of *Gtrgeo22* mRNA, it seems unlikely that GTRGEO22 is a reiterated component of the spermatid flagellum, as is the case for the product of the neighboring *Basigin* gene. Moreover, on the basis of the absence of significant neuronal defects in the CNS of ROSA22 mutants, it seems unlikely that GTRGEO22 is required for general axonal stability within neurons. Indeed, no generalized defect was observed in axonal transport in ROSA22 mutants in areas of the CNS expressing *Gtrgeo22* as evidenced by a normal pattern of immunohistochemical staining of arginine vasopressin being transported from the PVN to the posterior pituitary (L. J. Young, unpublished observations). The rationale for studying both sperm flagellar development and the basis for loss of intermale aggression in these mice is that, by doing so, a common function of *Gtrgeo22* may be elucidated more easily than by studying either process alone. We speculate that one possible common function of GTRGEO22 in development of the spermatid flagellum and facilitation of intermale aggressive behavior could involve sorting of specific proteins to a specialized subcellular compartment—*i.e.*, the developing flagellum in spermatids and the dendrites, axons, or even cell body in neurons. In this scenario, *Gtrgeo22* might encode an adaptor or adaptor-associated protein that is involved in linking specific protein cargo to molecular motors.

We thank J. Chamberlain for cDNA libraries, L. Melson for EM, and P. Soriano for the gift of ROSA22 mice. G.M. dedicates this work to the memory of Lonnie Russell, a masterful morphologist of spermatogenesis. This work was supported by grants from the National Institutes of Health (MH-00841 and DK-35254 to T.J.B, NS-32130 to M.B., HD-35494 to L.D.R., and HD-36437 to G.R.M.).

LITERATURE CITED

Altschul, S. F., W. Gish, W. Miller, E. W. Myers and D. J. Lipman, 1990 Basic local alignment search tool. J. Mol. Biol. **215:** 403–410.

Ausubel, F. M., R. Brent, R. E. Kingston, D. D. Moore, J. G. Seidman *et al.*, 1994 *Current Protocols in Molecular Biology*. Wiley Interscience, Boston.

Barkley, M. S., and B. D. Goldman, 1977 The effects of castration and Silastic implants of testosterone on intermale aggression in the mouse. Horm. Behav. **9:** 32–48.

Bartness, T. J., 1987 Animal body and fat changes: measurement and interpretation, pp. 463–498 in *Methods and Techniques to Study Feeding and Drinking Behavior*, edited by F. M. Toates and N. E. Rowland. Elsevier, Amsterdam.

Beeman, E. A., 1947 The effect of male hormone on aggressive behavior in mice. Physiol. Zool. **20:** 373–405.

Briskin, M. J., L. M. McEvoy and E. C. Butcher, 1993 MAdCAM-1 has homology to immunoglobulin and mucin-like adhesion receptors and to IgA1. Nature **363:** 461–464.

Carrera, A., G. L. Gerton and S. B. Moss, 1994 The major fibrous sheath polypeptide of mouse sperm: structural and functional similarities to the A-kinase anchoring proteins. Dev. Biol. **165:** 272–284.

Cebra-Thomas, J., and L. M. Silver, 1991 Genetic aspects of sperm differentiation and function in the mouse, pp. 29–56 in *Elements of Mammalian Fertilization*, edited by P. M. Wassarman. CRC Press, Boca Raton, FL.

Cole, D. G., D. R. Diener, A. L. Himelblau, P. L. Beech, J. C. Fuster *et al.*, 1998 Chlamydomonas kinesin-II-dependent intraflagellar transport (IFT): IFT particles contain proteins required for ciliary assembly in Caenorhabditis elegans sensory neurons. J. Cell Biol. **141:** 993–1008.

Davis, M., 1997 Neurobiology of fear responses: the role of the amygdala. J. Neuropsychiatry Clin. Neurosci. **9:** 382–402.

Demas, G. E., L. J. Kriegsfeld, S. Blackshaw, P. Huang, S. C. Gammie *et al.*, 1999 Elimination of aggressive behavior in male mice lacking endothelial nitric oxide synthase. J. Neurosci. **19:** RC30.

Dutcher, S. K., 1995 Flagellar assembly in two hundred and fifty easy-to-follow steps. Trends Genet. **11:** 398–404.

Fawcett, D. W., 1975 The mammalian spermatozoon. Dev. Biol. **44:** 394–436.

Fossella, J., S. A. Samant, L. M. Silver, S. M. King, K. T. Vaughan *et al.*, 2000 An axonemal dynein at the hybrid sterility 6 locus: implications for t haplotype-specific male sterility and the evolution of species barriers. Mamm. Genome **11:** 8–15.

Franklin, K. B. J., and G. Paxinos, 1997 *The Mouse Brain in Stereotaxic Coordinates*. Academic Press, San Diego.

Friedrich, G., and P. Soriano, 1991 Promoter traps in embryonic stem cells: a genetic screen to identify and mutate developmental genes in mice. Genes Dev. **5:** 1513–1523.

Fulcher, K. D., C. Mori, J. E. Welch, D. A. O'Brien, D. G. Klapper *et al.*, 1995 Characterization of Fsc1 cDNA for a mouse sperm fibrous sheath component. Biol. Reprod. **52:** 41–49.

Gandelman, R., 1972 Mice: postpartum aggression elicited by the presence of an intruder. Horm. Behav. **3:** 23–28.

Gerton, G. L., and C. F. Millette, 1984 Generation of flagella by cultured mouse spermatids. J. Cell Biol. **98:** 619–628.

Grant, E., and J. Mackintosh, 1963 A comparison of the social postures of some laboratory rodents. Behaviour **21:** 246–259.

Grijalva, C. V., E. D. Levin, M. Morgan, B. Roland and F. C.

Martin, 1990 Contrasting effects of centromedial and basolateral amygdaloid lesions on stress-related responses in the rat. Physiol. Behav. **48:** 495–500.

Handel, M.-A., 1987 Genetic control of spermatogenesis in mice, pp. 1–62 in *Results and Problems in Cell Differentiation-Spermatogenesis: Genetic Aspects*, edited by W. Hennig. Springer-Verlag, Berlin.

Heilker, R., M. Spiess and P. Crottet, 1999 Recognition of sorting signals by clathrin adaptors. Bioessays **21:** 558–567.

Hofmann, K., and W. Stoffel, 1993 TMbase—a database of membrane spanning protein segments. Biol. Chem. Hoppe-Seyler **347:** 166–176.

Hogan, B. L. M., R. S. P. Beddington, F. Costantini and E. Lacy, 1994 *Manipulating the Mouse Embryo: A Laboratory Manual.* Cold Spring Harbor Laboratory Press, Cold Spring Harbor, NY.

Huang, B., Z. Ramanis, S. K. Dutcher and D. J. Luck, 1982 Uniflagellar mutants of Chlamydomonas: evidence for the role of basal bodies in transmission of positional information. Cell **29:** 745–753.

Irons, M. J., and Y. Clermont, 1982a Formation of the outer dense fibers during spermiogenesis in the rat. Anat. Rec. **202:** 463–471.

Irons, M. J., and Y. Clermont, 1982b Kinetics of fibrous sheath formation in the rat spermatid. Am. J. Anat. **165:** 121–130.

Kagami, O., M. Gotoh, Y. Makino, H. Mohri, R. Kamiya *et al.*, 1998 A dynein light chain of sea urchin sperm flagella is a homolog of mouse Tctex 1, which is encoded by a gene of the t complex sterility locus. Gene **211:** 383–386.

Kozak, M., 1987 An analysis of 5′-noncoding sequences from 699 vertebrate messenger RNAs. Nucleic Acids Res. **15:** 8125–8148.

Kozminski, K. G., P. L. Beech and J. L. Rosenbaum, 1995 The Chlamydomonas kinesin-like protein FLA10 is involved in motility associated with the flagellar membrane. J. Cell Biol. **131:** 1517–1527.

LeDoux, J. E., 2000 Emotion circuits in the brain. Annu. Rev. Neurosci. **23:** 155–184.

Leestma, J. E., and S. Sepsenwol, 1980 Sperm tail axoneme alterations in the Wobbler mouse. J. Reprod. Fertil. **58:** 267–270.

Leshner, A. I., V. A. Litwin and R. L. Squibb, 1972 A simple method for carcass analysis. Physiol. Behav. **9:** 281–282.

MacGregor, G. R., B. P. Zambrowicz and P. Soriano, 1995 Tissue non-specific alkaline phosphatase is expressed in both embryonic and extraembryonic lineages during mouse embryogenesis but is not required for migration of primordial germ cells. Development **121:** 1487–1496.

Maruniak, J. A., C. J. Wysocki and J. A. Taylor, 1986 Mediation of male mouse urine marking and aggression by the vomeronasal organ. Physiol. Behav. **37:** 655–657.

Mitchell, D. R., 2000 *Chlamydomonas* flagella. J. Phycology **36:** 261–273.

Mortimer, S. T., 1997 A critical review of the physiological importance and analysis of sperm movement in mammals. Hum. Reprod. Update **3:** 403–439.

Nebel, B. R., A. P. Amarose and E. M. Hackett, 1961 Calendar of gametogenic development in the prepubertal male mouse. Science **134:** 832–833.

Neilson, L. I., P. A. Schneider, P. G. Van Deerlin, M. Kiriakidou, D. A. Driscoll *et al.*, 1999 cDNA cloning and characterization of a human sperm antigen (SPAG6) with homology to the product of the Chlamydomonas PF16 locus. Genomics **60:** 272–280.

Nelson, R. J., and S. Chiavegatto, 2001 Molecular basis of aggression. Trends Neurosci. **24:** 713–719.

Nelson, R. J., G. E. Demas, P. L. Huang, M. C. Fishman, V. L. Dawson *et al.*, 1995 Behavioural abnormalities in male mice lacking neuronal nitric oxide synthase. Nature **378:** 383–386.

O'Brien, D. A., and A. R. Bellve, 1980 Protein constituents of the mouse spermatozoon. I. An electrophoretic characterization. Dev. Biol. **75:** 386–404.

O'Bryan, M. K., K. L. Loveland, D. Herszfeld, J. R. McFarlane, M. T. Hearn *et al.*, 1998 Identification of a rat testis-specific gene encoding a potential rat outer dense fibre protein. Mol. Reprod. Dev. **50:** 313–322.

Ogawa, S., D. B. Lubahn, K. S. Korach and D. W. Pfaff, 1997 Behavioral effects of estrogen receptor gene disruption in male mice. Proc. Natl. Acad. Sci. USA **94:** 1476–1481.

Olson, E. N., H. H. Arnold, P. W. Rigby and B. J. Wold, 1996 Know your neighbors: three phenotypes in null mutants of the myogenic bHLH gene MRF4. Cell **85:** 1–4.

Patel-King, R. S., S. E. Benashski, A. Harrison and S. M. King, 1997 A Chlamydomonas homologue of the putative murine t complex distorter Tctex-2 is an outer arm dynein light chain. J. Cell Biol. **137:** 1081–1090.

Pazour, G. J., C. G. Wilkerson and G. B. Witman, 1998 A dynein light chain is essential for the retrograde particle movement of intraflagellar transport (IFT). J. Cell Biol. **141:** 979–992.

Pazour, G. J., B. L. Dickert and G. B. Witman, 1999 The DHC1b (DHC2) isoform of cytoplasmic dynein is required for flagellar assembly. J. Cell Biol. **144:** 473–481.

Phillips, D. M., 1974 *Spermiogenesis.* Academic Press, New York.

Phillips, D. M., S. H. Pilder, P. J. Olds-Clarke and L. M. Silver, 1993 Factors that may regulate assembly of the mammalian sperm tail deduced from a mouse t complex mutation. Biol. Reprod. **49:** 1347–1352.

Pilder, S., and S. A. Samant, 2001 The *hybrid sterility 6* locus: a model system for studying sperm tail-related infertility in humans, pp. 317–326 in *Andrology in the 21st Century: Proceedings of the VIIth International Congress of Andrology*, edited by B. Robaire, H. Chemes and C. Morles. Medimond, Englewood, NJ.

Pilder, S. H., P. Olds-Clarke, D. M. Phillips and L. M. Silver, 1993 Hybrid sterility-6: a mouse t complex locus controlling sperm flagellar assembly and movement. Dev. Biol. **159:** 631–642.

Plon, S. E., K. A. Leppig, H. N. Do and M. Groudine, 1993 Cloning of the human homolog of the CDC34 cell cycle gene by complementation in yeast. Proc. Natl. Acad. Sci. USA **90:** 10484–10488.

Porter, M. E., R. Bower, J. A. Knott, P. Byrd and W. Dentler, 1999 Cytoplasmic dynein heavy chain 1b is required for flagellar assembly in Chlamydomonas. Mol. Biol. Cell **10:** 693–712.

Rosenbaum, J. L., D. G. Cole and D. R. Diener, 1999 Intraflagellar transport: the eyes have it. J. Cell Biol. **144:** 385–388.

Ross, A. J., K. G. Waymire, J. E. Moss, A. F. Parlow, M. K. Skinner *et al.*, 1998 Testicular degeneration in Bclw-deficient mice. Nat. Genet. **18:** 251–256.

Rost, B., 1996 PHD: predicting one-dimensional protein structure by profile-based neural networks. Methods Enzymol. **266:** 525–539.

Rowe, F. A., and D. A. Edwards, 1971 Olfactory bulb removal: influences on the aggressive behaviors of male mice. Physiol. Behav. **7:** 889–892.

Rowe, L. B., J. H. Nadeau, R. Turner, W. N. Frankel, V. A. Letts *et al.*, 1994 Maps from two interspecific backcross DNA panels available as a community genetic mapping resource. Mamm. Genome **5:** 253–274.

Russell, L. D., R. A. Ettlin, A. P. Sinha Hikim and E. D. Clegg, 1990 *Histological and Histopathological Evaluation of the Testis.* Cache River Press, Clearwater, FL.

Sampson, M. J., W. K. Decker, A. L. Beaudet, W. Ruitenbeek, D. Armstrong *et al.*, 2001 Immotile sperm and infertility in mice lacking mitochondrial voltage-dependent anion channel type 3. J. Biol. Chem. **276:** 39206–39212.

Shao, X., J. Xue and F. A. van der Hoorn, 2001 Testicular protein Spag5 has similarity to mitotic spindle protein Deepest and binds outer dense fiber protein Odf1. Mol. Reprod. Dev. **59:** 410–416.

Stowers, L., T. E. Holy, M. Meister, C. Dulac and G. Koentges, 2002 Loss of sex discrimination and male-male aggression in mice deficient for TRP2. Science **295:** 1493–1500.

Van Oortmerssen, G. A., D. J. Dijk and T. Schuurman, 1987 Studies in wild house mice. II. Testosterone and aggression. Horm. Behav. **21:** 139–152.

Wang, Z. X., Y. Liu, L. J. Young and T. R. Insel, 2000 Hypothalamic vasopressin gene expression increases in both males and females postpartum in a biparental rodent. J. Neuroendocrinol. **12:** 111–120.

Communicating editor: C. Kozak